JOURNAL OF GEOPHYSICAL RESEARCH, VOL. 104, NO. D3, PAGES 3729-3739, FEBRUARY 20, 1999

# Diurnal variations in the middle atmosphere observed by UARS

Fabrizio Sassi

Atmospheric Systems and Analysis, Westminster, Colorado

Murry Salby

Program in Atmospheric and Ocean Sciences, University of Colorado, Boulder

**Abstract.** This paper investigates diurnal variations in the dynamical and chemical structure of the middle atmosphere observed by UARS. Dynamical variations are of tidal nature and appear prominently in the temperature field near the equator. The temperature field is smooth enough for higher harmonics of the diurnal cycle, which are unresolved by the UARS sampling, to be negligible. Diurnal variations in the temperature field can therefore be mapped synoptically. Daily maps of the diurnal variation of temperature exhibit meridional and vertical structure typical of the propagating solar diurnal tide. Through advective and photochemical effects, diurnal variations of temperature introduce diurnal variations of ozone in the middle and upper stratosphere, chemical variations which are mapped in similar fashion. Diurnal variations of other chemical species contain higher harmonics, which are undersampled by UARS, preventing diurnal variations in those species from being mapped reliably. Instead, the average diurnal variation over a month or longer is composited from observations at individual local times. In the middle stratosphere, diurnal variations of $NO_x$ are strongly influenced by the zonal mean distribution of $NO_x$, which in turn is controlled by the mean meridional circulation. So too are diurnal variations of $ClO_x$ but with sign opposite to those of $NO_x$, owing to the coupling of those families.

## 1. Introduction

Diurnal variations in the middle atmosphere occur through tidal oscillations in thermal and wind fields and as variations of photochemically active constituents. Diurnal tides [*Lindzen*, 1967; *Forbes*, 1982] are forced thermally through radiative absorption by water vapor and ozone. The propagating component of the tide, while small in amplitude at lower levels, grows rapidly with elevation and becomes prominent in upper portions of the middle atmosphere. At the same time, the diurnal cycle of solar insolation affects chemical species whose abundances are determined by photochemical production and destruction. Although the diurnal cycle of chemical species is predominant at higher levels, some constituents have larger concentrations in the middle and lower stratosphere, where the impact of their diurnal variation on local chemistry is greater.

Several observations suggest that the migrating diurnal tide in the mesosphere is stronger at equinox than at solstice [*Vincent et al.*, 1988; *Burrage et al.*, 1995; *McLandress et al.*, 1996]. Since the migrating tide is a prominent dynamical feature in upper portions of the middle atmosphere, its structure and variability are relevant to modelling studies. Thus far, however, the origin of its seasonal variation remains unknown.



Paper number 1998JD100068.
0148-0227/99/1998JD100068$09.00

Satellites provide information on the dynamical, thermal, and chemical structure of the middle atmosphere. Polar-orbiting satellites are Sun synchronous: They sample different longitudes at the same local time and therefore at the same phase of the diurnal cycle. Consequently, they provide very limited information on westward migrating diurnal variations, namely, day-night differences of field properties [e.g., *Hitchman and Leovy*, 1985]. On the other hand, eastward migrating diurnal tides are fully resolved and have been studied previously [e.g., *Lieberman*, 1991].

To fully describe diurnal variations, it is necessary to sample a field property at all local times. The Upper Atmosphere Research Satellite (UARS) has a medium-inclination orbit (57°) that precesses through local time. Because it samples the Earth slightly faster than once per day, this orbit pushes the Nyquist limit of asynoptic sampling [*Salby*, 1982a] just beyond 1.0 cpd. If no significant variance lies beyond this Nyquist limit, it is then possible to synoptically map the field property and, in particular, its diurnal variation.

Diurnal variations in field properties observed by UARS are studied here with Fast Fourier Synoptic Mapping (FFSM), which makes full use of the information content of the asynoptic measurements [*Salby*, 1982b). Temperature, because it tends to be the smoothest, is the field property whose diurnal variation is best observed by UARS. Moreover, temperature is measured simultaneously by several instruments on board UARS. This feature allows long records to be mapped and reduces the statistical error in the final products [*Sassi*

*and Salby*, 1998]. Chemical variations, on the other hand, can involve space scales and timescales beyond the Nyquist limits of asynoptic sampling by single orbiting platform [*Salby*, 1988]. Space scales and timescales are undersampled if a constituent changes abruptly. For example, a photochemically active species contains a prominent diurnal variation with sudden changes at dusk and dawn. Such changes introduce higher harmonics of the diurnal cycle, which are undersampled by UARS, preventing the diurnal variation from being mapped synoptically. Even then, however, the precessing orbit of UARS allows an average diurnal variation to be composited by collecting local times over a month or longer.

In section 2 we describe the data and method of analysis employed in this study. Diurnal variations of temperature, associated with tidal oscillations, are recovered in section 3 from the temperature space-time spectrum and then validated against independent evidence. Section 4 presents diurnal variations of chemical constituents, which are composited as averages over a few UARS yaw periods. Conclusions are drawn in section 5.

## 2. Data and Methods of Analysis

The starting point for this study is level 3AL data from UARS. These data are asynoptic observations along the viewing track, interpolated every 4° of latitude between 80°S and 80°N at standard pressure levels. The 3AL data are mapped synoptically via FFSM from which diurnal variations are available.

### 2.1. Analysis of Dynamical Oscillations

Tidal oscillations are a prominent feature of the temperature field in the tropics [*Chapman and Lindzen*, 1970]. The gravest harmonic is sampled properly by UARS, so long as higher harmonics are absent. This requirement is satisfied by the propagating mode of the diurnal tide, since semidiurnal variability is, to a large extent, vertically trapped near its source [*Chapman and Lindzen*, 1970].

Field properties have been mapped synoptically using the operational algorithm developed by *Sassi and Salby* [1998]. The algorithm makes use of contemporaneous measurements of an individual field property by different UARS instruments. Temperature is simultaneously measured by the Cryogenic Limb Array Etalon Spectrometer (CLAES) (Version 7), the Improved Stratospheric and Mesospheric Sounder (ISAMS) (Version 8), and the Microwave Limb Sounder (MLS) (Version 3). Simultaneous measurements from these instruments greatly reduce the number and length of data gaps, achieving greater statistical confidence in the combined products. The remaining gaps, a day or shorter, are interpolated using a two-dimensional (2-D) convolver. The combined asynoptic data are then mapped synoptically using FFSM and a signal-to-noise threshold that rejects random error exceeding a 10% rms level.

An intermediate product of the synoptic mapping procedure is the space-time spectrum of the observed field. Figure 1 shows the wavenumber 1 frequency

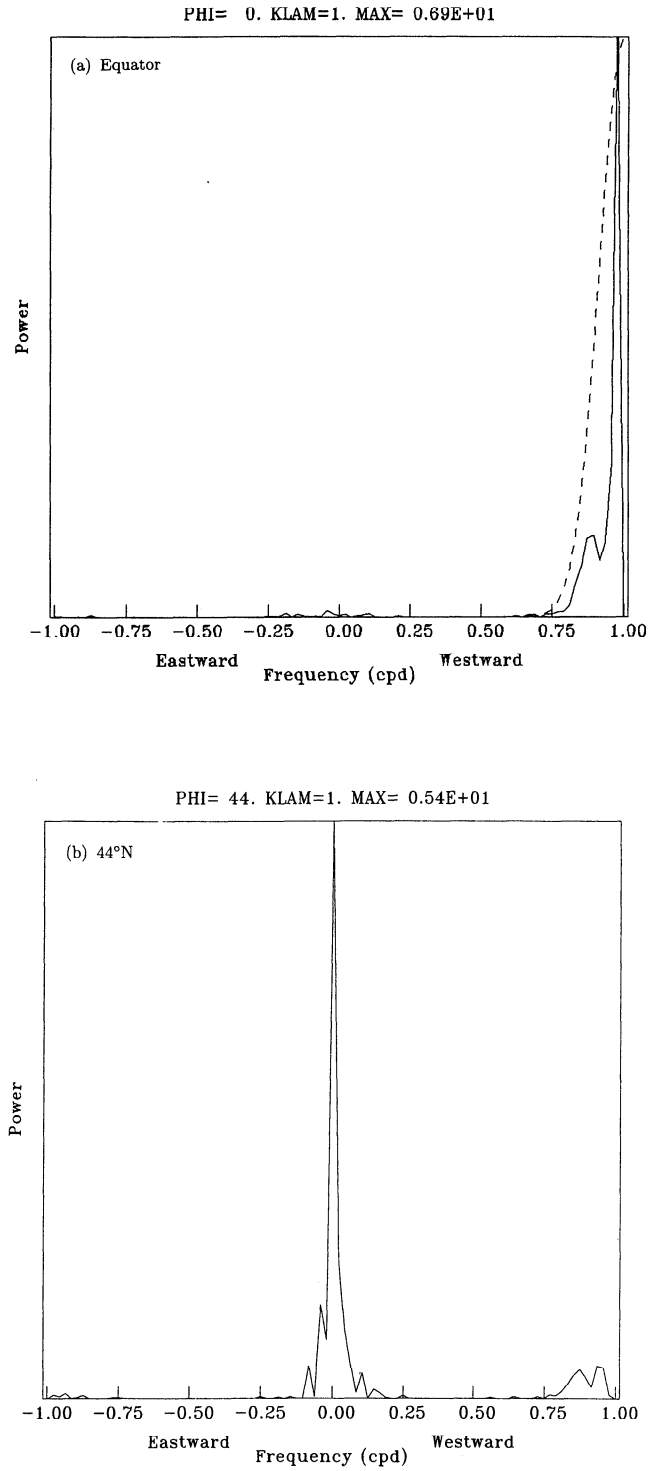


**Figure 1.** Space-time power spectrum of temperature zonal wavenumber (KLAM) 1 at 1 hPa for (a) the equator (PHI=0) and (b) 44°N (PHI=44). The spectrum was computed from simultaneous observations of CLAES, ISAMS and MLS made during a northward looking orbit, from February 15, 1992, to March 22, 1992. The dashed line in Figure 1a indicates the high-pass filter used to isolate the diurnal variations at wavenumber 1. Variance of the largest spectral component is reported in the top label (MAX).

spectrum of temperature at 1 hPa. The spectrum corresponds to observations made during a northward looking yaw period, from February 15, 1992, to March 22, 1992. At the equator (Figure 1a) the westward propagating diurnal oscillation is a prominent feature of the spectrum: Power (solid line) peaks at ~1.0 cpd and decreases rapidly at smaller frequencies. (The diurnal peak is removed slightly from 1.0 cpd because UARS does not complete an integer number of orbits in an integer number of days.) No appreciable power is present at frequencies smaller than 0.75 cpd. It should be noted that the diurnal variation of temperature is particularly large during spring 1992. At other times (not shown) the zonal wavenumber 1 spectrum of temperature also contains low-frequency variance, which has been identified with Kelvin waves [e.g., *Canziani et al.*, 1994]. For instance, during December 1991, when equatorial wind in the upper stratosphere is easterly, the spectrum of equatorial temperature also exhibits low-frequency Kelvin wave activity, with variance comparable to or greater than the diurnal tide. At midlatitudes (Figure 1b), on the other hand, the spectrum of wavenumber 1 is characterized by low-frequency variability, with a tidal oscillation that is still visible but comparatively small.

The Nyquist frequency for UARS sampling lies just beyond 1.0 cpd. Consequently, the first harmonic of the diurnal cycle is marginally resolved. (It is worth noting that the mapping procedure does not require linearity, steady state, or even statistical stationarity of the observed behavior, as is demonstrated by *Salby* [1982b], considerations that would be violated, for example, by interaction between the tide and planetary waves. So long as the field is adequately sampled, FFSM recovers the true synoptic behavior.) Higher harmonics, however, are not resolved and, if present, alias other space scales and timescales recovered by the mapping procedure [*Salby and Callaghan*, 1997; *Sassi and Salby*, 1999]. In order to verify whether higher harmonics of the diurnal cycle are present, we make use of the sampling characteristics of UARS to composite an average diurnal variation that includes all diurnal harmonics. The UARS orbit retrogresses about the Earth at a rate slightly faster than $2\pi$ rad $d^{-1}$, so at a given latitude, different local times are sampled on different days. Implications of the UARS orbit appear in Figure 2, which plots the local time (LT) of the ascending and descending crossings at the equator (Figure 2a) and at 76°S (Figure 2b), each during a southward looking yaw period. The coverage of local time during a single yaw period is seen to be incomplete, with some local times left unsampled. This shortcoming is pronounced at high latitudes (Figure 2b), where the combined sampling covers little more than half of the day (~15 hours). In fact, the coverage of local time is marginally complete after one yaw period only between 32°S and 48°S (not shown). Even there the number of observations is limited, leaving gaps of LT, as well as large difference in population number between bins of LT.

The precessing nature of the sampling allows observations at individual local times to be averaged to form a "composite diurnal variation" of a field property. In practice, observations must be averaged over a few yaw periods (e.g., 1-3 months) to fully populate all bins of LT, as is evident from Figure 2. The composite diurnal variation then represents only the mean daily variation over the entire averaging interval. A composite diurnal variation is formed by collecting all observations at a given latitude and level in bins of 2 hours of LT. To obtain a global composite, we averaged observations over as many as three yaw periods.

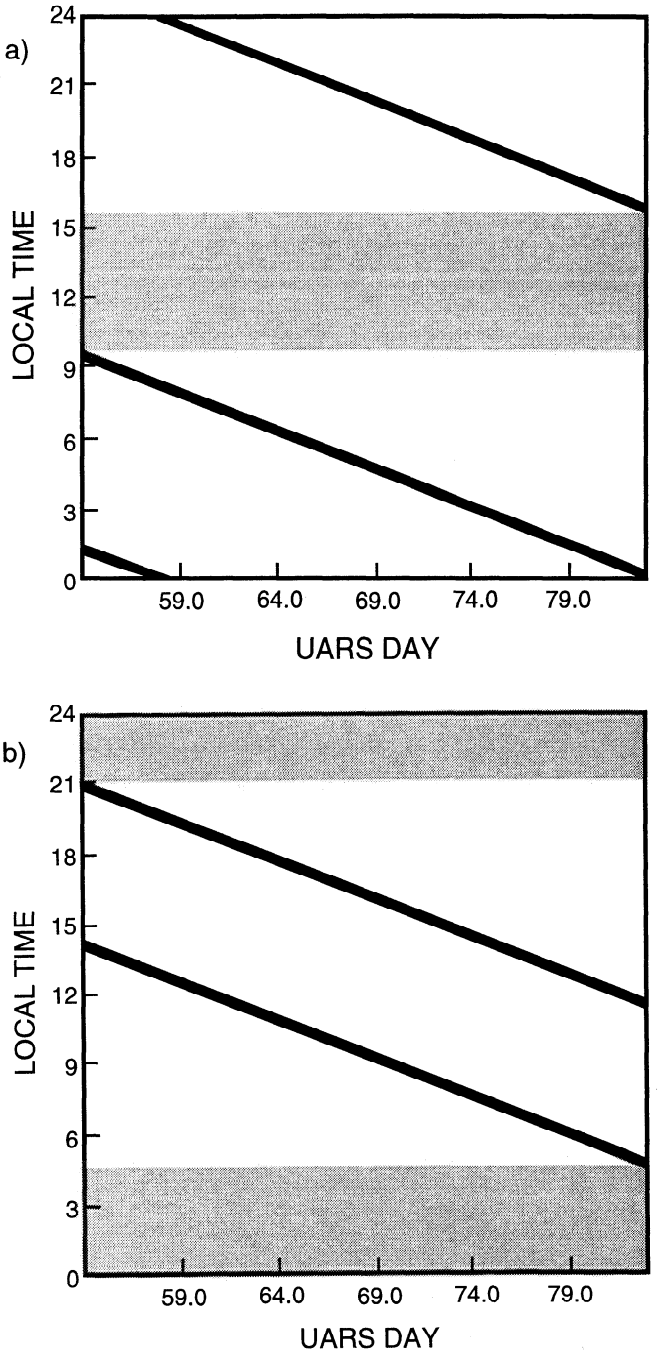


**Figure 2.** Local time (LT) of observations made during a southward looking orbit at (a) the equator and (b) at 76°S. UARS day is the day from the beginning of the satellite mission. Shading indicates the range of LT that is not being sampled.

The statistical significance of the composite diurnal variation is evaluated in terms of the rms deviation for

each bin of LT and for each latitude and height. For a population of $N$ observations the rms deviation from the mean obeys a $\chi^2$ probability distribution. Requiring this probability to be smaller than 10% requires that the population be sharply clustered about its mean, which then clearly defines the diurnal value at that LT. Only LT bins satisfying this criterion are included in the composite diurnal variation.

Figure 3 shows the composite diurnal variation of equatorial temperature (with the mean subtracted out), obtained by averaging all observations at 2-hour intervals of LT from February 15, 1992, to March 22, 1992. At 10 hPa the composite diurnal variation is dominated by the first harmonic (i.e., by a period of 24 hours), which has an amplitude of ~2 K. This is, in fact, comparable to Kelvin wave oscillations at this level that have been observed at other times of the year [e.g., *Salby et al.*, 1984; *Canziani et al.*, 1994]. The largest temperature occurs at ~20 LT, and the smallest occurs at ~10 LT. The departure from a simple harmonic oscillation in early hours of the day reflects the presence of higher diurnal harmonics. At 1 hPa the composite diurnal variation is still dominanted by the first harmonic. However, the spike appearing around midday also introduces higher harmonics.

Figure 3 illustrates the prevalence of the first harmonic in the tropics, consistent with classical tidal theory [*Chapman and Lindzen*, 1970]. However, higher harmonics are also present in the composite diurnal variation of temperature, in particular, at higher levels. At 1 hPa, higher harmonics of the diurnal cycle account for ~30% of the amplitude in Figure 3. Although they are undersampled by UARS, those higher diurnal harmonics represent a small fraction of the total variance of temperature, which can then be mapped synoptically.

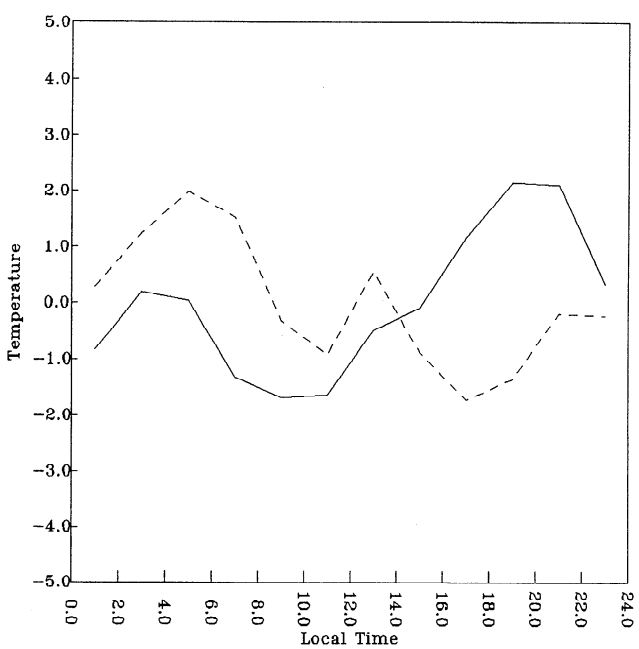


**Figure 3.** Composite diurnal cycle of temperature, averaged at 2-hour intervals of local time, from February 15, 1992, to March 22, 1992. The solid line is the temperature at 10 hPa; dashed line s the temperature at 1 hPa. At both levels, the mean of the diurn al cycle was subtracted out.

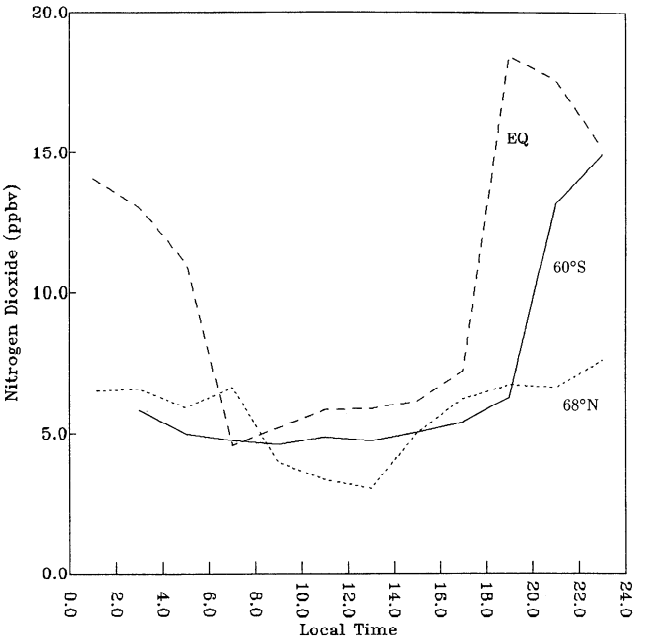


**Figure 4.** Composite diurnal cycle of nitrogen dioxide (in ppbv), averaged at 2-hour intervals of local time, from November 3, 1991, to February 13, 1992. The solid line is the composite over 60°S, the dashed line is the composite over the equator, and the dotted line is the composite over 68°N. Composite was obtained by using observations made by ISAMS.

## 2.2. Analysis of Chemical Oscillations

Unlike temperature, chemical species that are photochemically active (i.e., have short photochemical lifetimes) can have a diurnal variation that is a substantial fraction of the total variance. Figure 4 shows the composite diurnal variation of $NO_2$ at 5 hPa over 60°S, the equator, and 68°N, which was formed by averaging measurements from November 3, 1991, to February 13, 1992. Nitrogen dioxide is rapidly dissociated in sunlight. At the high summer latitude 60°S, the $NO_2$ mixing ratio is small throughout most of the day, except for only a few hours after sunset, when it increases sharply to values approaching 15 ppbv. This sharp transition introduces higher harmonics of the diurnal cycle. Involving periods of 12 hours, 8 hours, etc., these higher harmonics are undersampled by UARS. The higher diurnal harmonics have amplitudes comparable to the mean. Higher harmonics are also introduced by the uneven nature of the diurnal cycle at 60°S, which mirrors the uneven length of day and night over the summer pole. Over the equator the diurnal variation is evenly distributed in LT, positive and negative anomalies each occupying ~12 hours. However, the transitions between daytime and nighttime values are quite sharp and are about as large as the mean. At 68°N the depression of $NO_2$ during daylight is limited to 6 hours, with a more gradual recovery to higher nighttime values dragging on beyond

14 LT. As at 60°S, the uneven change between day and night at high winter latitudes introduces higher diurnal harmonics that are undersampled by UARS.

The presence of appreciable variance beyond the Nyquist limit of asynoptic sampling prevents the diurnal variation of short-lived chemical species like $NO_2$ from being mapped to recover the instantaneous record. The diurnal variation of such species is therefore treated only as a time-mean composite, like that shown in Figure 4, which represents an average diurnal variation over several UARS yaw periods.

## 3. Dynamical Variations

### 3.1. Tidal Oscillations

Diurnal temperature variations are apparent throughout the tropics. Diurnal power is broadly distributed about 1.0 cpd (see Figure 1) and, depending on the height and time of year, the diurnal variation can be a substantial part of the total variance. The high-pass frequency filter, superposed in Figure 1a, recovers the temperature diurnal variance.

The space-time spectrum is filtered according to Figure 1 to compute synoptic daily maps of the diurnal variation of temperature. The map for 10 hPa is shown in Figure 5 at 0000 Greenwich Mean Time (GMT) on March 3, 1992 (day 63), when UARS was viewing northward. The temperature oscillation maximizes at 1.1 K, just off the equator at 12°N. Maximum temperature occurs at 20 LT, as in the composite diurnal variation in Figure 3. There is a phase reversal at 30°N, with amplitudes poleward being about half of tropical amplitudes. The meridional structure in Figure 5 is very similar to that of the fundamental Hough mode as it appears in numerical calculations of the tide [e.g., *Chapman and Lindzen*, 1970]. Diurnal amplitudes in Figure 5 are eventually limited by the asynoptic sampling of UARS near the highest latitudes observed, where ascending and descending observations converge and therefore cease to be independent. To account for the reduced information content at those latitudes, the space-time spectrum is low-pass filtered, with a cutoff frequency that decreases to 0.5 cpd by the extreme latitudes [*Sassi and Salby*, 1998].

The amplitude and phase of the diurnal oscillation in Figure 5 are broadly consistent with theoretical calculations of the solar diurnal tide. *Lindzen's* [1967] numerical solution yields an amplitude at the equator under equinox conditions of ~1 K at 30 km. Similar amplitudes were obtained by *McLandress* [1997] using the Canadian Middle Atmosphere Model. The temperature variation maximizes at ~15 LT in Lindzen's calculation but at 18-20 LT in McLandress' analysis, closer to that observed in Figures 5 and 3.

It is instructive to compare the daily map in Figure 5 against the composite at 10 hPa in Figure 3, which represents the average diurnal variation over the equator. The excursion of temperature in the composite diurnal variation indicates an amplitude of 1-2 K over the equator, whereas a maximum amplitude in the daily map of 1.1 K is found just north of the equator. These differences reflect day-to-day changes in the diurnal variation of temperature. They are represented in the space-time spectrum (e.g., Figure 1a), by a band of frequency about 1.0 cpd.

### 3.2. Tidal-Induced Chemical Oscillations

Vertical motion induced by tidal oscillations transports long-lived chemical species. *Chapman and Lindzen* [1970] show that near the equator the propagating mode is dominant and that there the vertical velocity field is largest. The effect of vertical motion will be greatest on a tracer with a large vertical gradient. Combining the equations of thermodynamics and continuity for a conservative tracer in the presence of only vertical advection [e.g., *Andrews et al.*, 1987] leads to a relationship between the diurnal amplitude of temperature $\hat{T}$ and tracer mixing ratio $\hat{\mu}$:

$$\hat{\mu} = \frac{R}{HN^2}\overline{\mu}_z\hat{T}, \tag{1}$$

where $\overline{\mu}_z$ is the zonal mean vertical gradient and $R$, $H$, and $N^2$ are the gas constant for dry air, the vertical scale height, and the square of the buoyancy frequency, respectively.

A tracer that satisfies the requirements leading to (1) is ozone below 10 hPa, where its lifetime is of

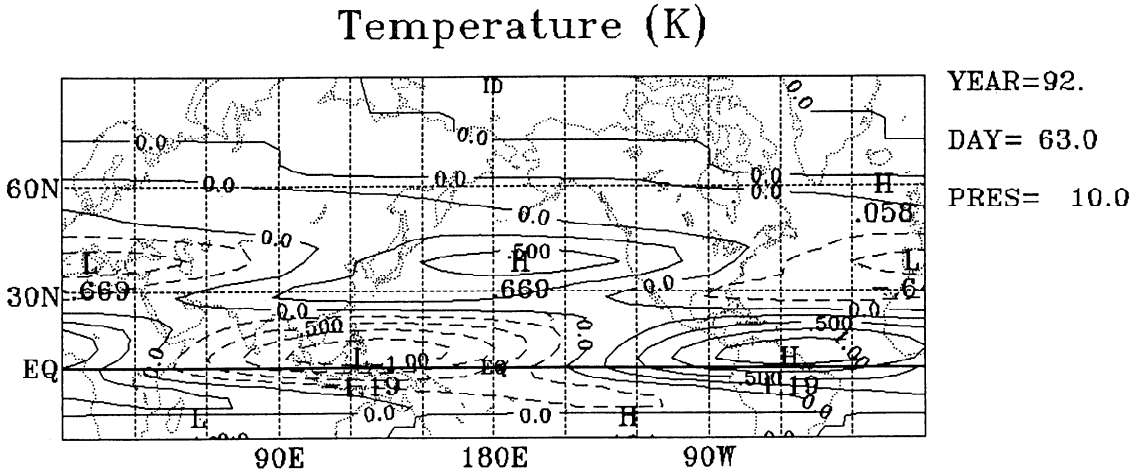


**Figure 5.** Zonal wavenumber 1 map for 10 hPa of filtered diurnal variation of temperature at 0000 GMT on March 3, 1992. The contour interval is 0.25 K.

the order of 10 days or longer [e.g., *Solomon et al.*, 1985]. Figure 6 shows the synoptic diurnal variations of temperature and ozone, each at 15 hPa, on the same day as that in Figure 5. The temperature anomaly (Figure 6a) maximizes at ~12°N with an amplitude of 0.6 K. Phase changes abruptly at 30°N, with amplitudes between 30°N and 60°N comparable to the tropical values. The diurnal variation of ozone (Figure 6b) shows a maximum amplitude of ~0.08 ppmv also at ~12°N, nearly in phase with the temperature anomaly. A phase reversal occurs at 30°N and poleward of this latitude, amplitudes are about half of the tropical values.

To verify that the diurnal ozone variability is of tidal origin, we use (1) to calculate the implied diurnal variation of a tracer. Using the temperature amplitude in Figure 6a and the zonal mean vertical gradient of ozone observed at the equator (not shown) yields an ozone amplitude of $\hat{\mu}$ ~0.06 ppmv, in reasonable agreement with the observed variation in Figure 6b. The small discrepancy in phase (2-3 hours) may reflect the following approximations: (1) The photochemical lifetime of ozone at 15 hPa over the equator is shorter than 10 days. Photochemical processes not accounted for can then alter the phase relation between the tracer and temperature by as much as 10%. (2) The anomalies in Figure 6 are both slightly north of the equator, where tidal meridional motion and corresponding transport increase rapidly with latitude.

Above 10 hPa, ozone is not a passive tracer since photochemistry operates on a timescale of only hours [e.g., *Brasseur and Solomon*, 1986]. In the upper stratosphere, ozone is in photochemical equilibrium, and its distribution is determined by incoming solar radiation and thermal structure. It is possible to relate the relative variation of ozone to the relative variation of temperature by assuming oxygen-only chemistry [*Brasseur and Solomon*, 1986], which leads to the following

$$\frac{\hat{\mu}}{\overline{\mu}} \simeq -5.6\frac{\hat{T}}{\overline{T}}, \tag{2}$$

where $\hat{\mu}$ and $\hat{T}$ are the ozone and temperature amplitudes, respectively, and $\overline{\mu}$ and $\overline{T}$ are the corresponding zonal mean values.

Figure 7 shows the diurnal variations of temperature and ozone at 1 hPa on the same day as that for Figure 5. At this level, the maximum temperature variation (Figure 7a) ~3.7 K and directly over the equator. A phase reversal occurs at ~15°N. The maximum amplitude

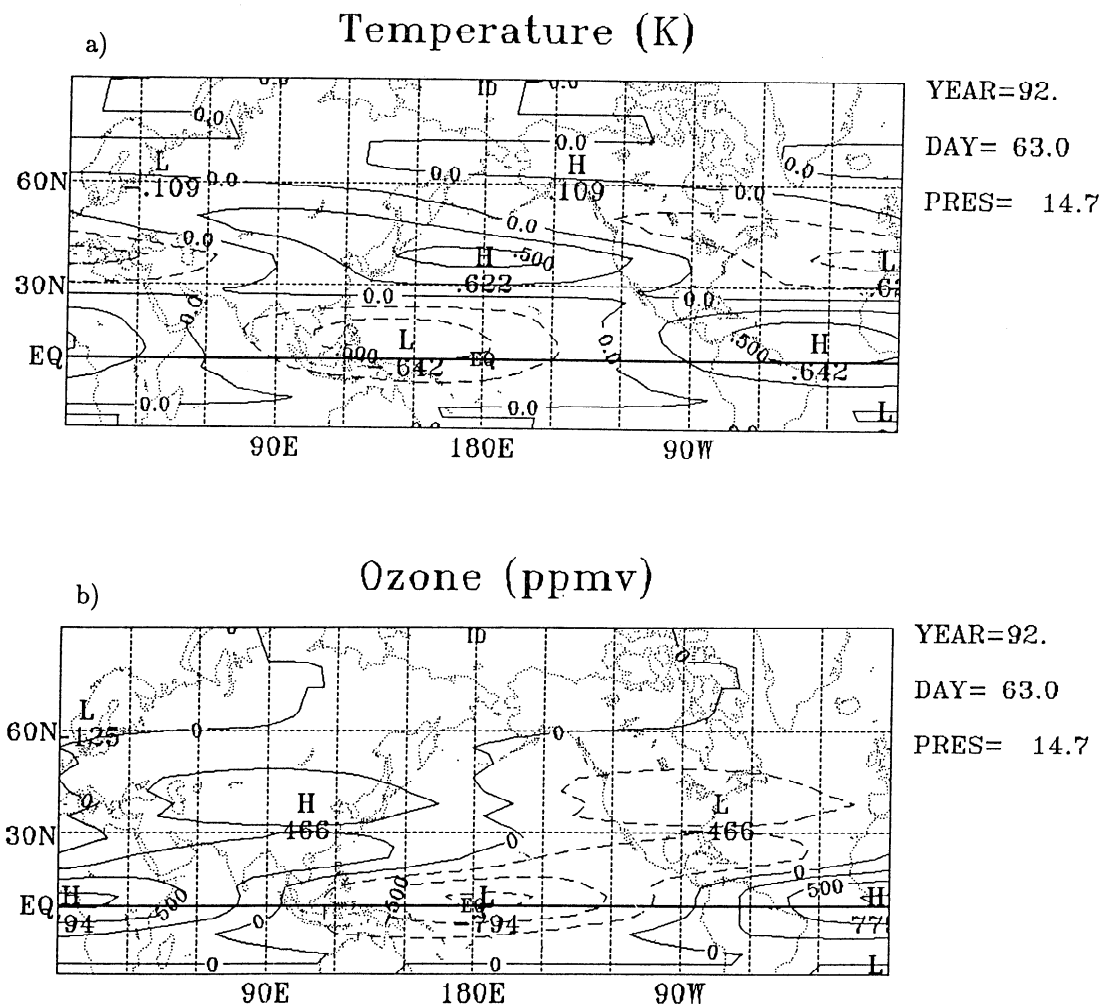


**Figure 6.** Zonal wavenumber 1 maps for 14.7 hPa of filtered diurnal variation of (a) temperature and (b) ozone, at 0000 GMT on March 3, 1992. The contour interval is 0.25 K in Figure 6a and 0.025 ppmv in Figure 6b.

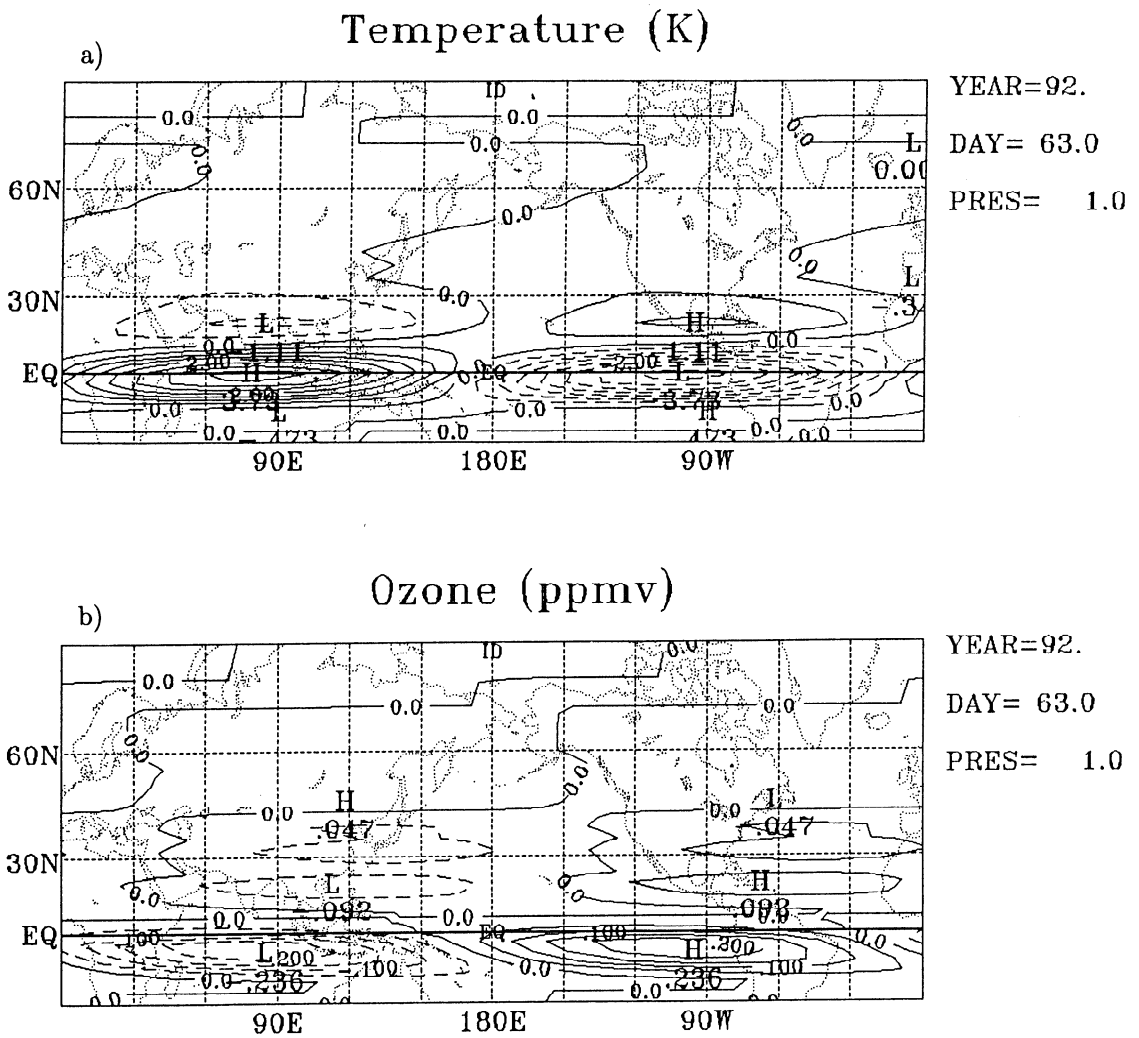


**Figure 7.** As in Figure 6 but at 1 hPa. The contour interval is 0.5 K in Figure 7a and 0.05 ppmv in Figure 7b.

occurs at ~6 LT. The phase difference between diurnal variations at the neighboring levels 1.5 and 0.7 hPa (not shown) implies a vertical wavelength of 22 km. This vertical structure is in accord with numerical calculations of the tide [*Lindzen*, 1967; *McLandress*, 1997].

The ozone anomaly (Figure 7b) maximizes just south of the equator, with an amplitude of ~0.2 ppmv. At this level, ozone and temperature anomalies have opposite phase. For typical values of $\overline{\mu}$, $\overline{T}$, and $\hat{T}$ at 1 hPa, (2) implies a diurnal amplitude of ozone of ~0.2 ppmv, in agreement with Figure 7b. The small meridional discrepancy in latitude between ozone and temperature may follow from rapid meridional changes of photodissociation rates, which are not accounted for by (2).

### 3.3. Seasonal Variations

The mean seasonal variation of the diurnal tide has been composited by averaging on individual days of the year diurnal variations over the first three years of the UARS mission (October 1991 through September 1994). Figure 8 shows the rms amplitude of the diurnal variation of temperature as a function of day and latitude between 28°S and 28°N. At 10 hPa (Figure 8a), maximum amplitude is attained in northern winter, when the diurnal variation exceeds 1 K at ~10N. In the Southern Hemisphere the amplitude of the diurnal variation is largest in June and July (~0.75 K), again during winter. The maximum temperature oscillation thus meanders across the equator opposite to solar heating. At 1 hPa (Figure 8b) the meridional excursion of the tide is much smaller, the amplitude maximum remaining close to the equator throughout the year. Amplifications still occur, however, being contemporaneous with those at lower levels. However, at this level, the temperature maximum is found on the opposite side of the equator at ~5°S in the summer hemisphere, coincident with solar heating. Through the seasonal amplifications that occur near each solstice, the tide's amplitude varies from ~0.5 K to more than 5 times as large.

A striking feature of the tide's seasonality is the excursion into opposite hemispheres in the middle stratosphere (Figure 8a) and upper stratosphere (Figure 8b). Similar behavior is evident in modeling calculations of the tide [*McLandress*, 1997; *Wu et al.*, 1998]. The reason for the seasonal meandering in opposite hemispheres in Figure 8

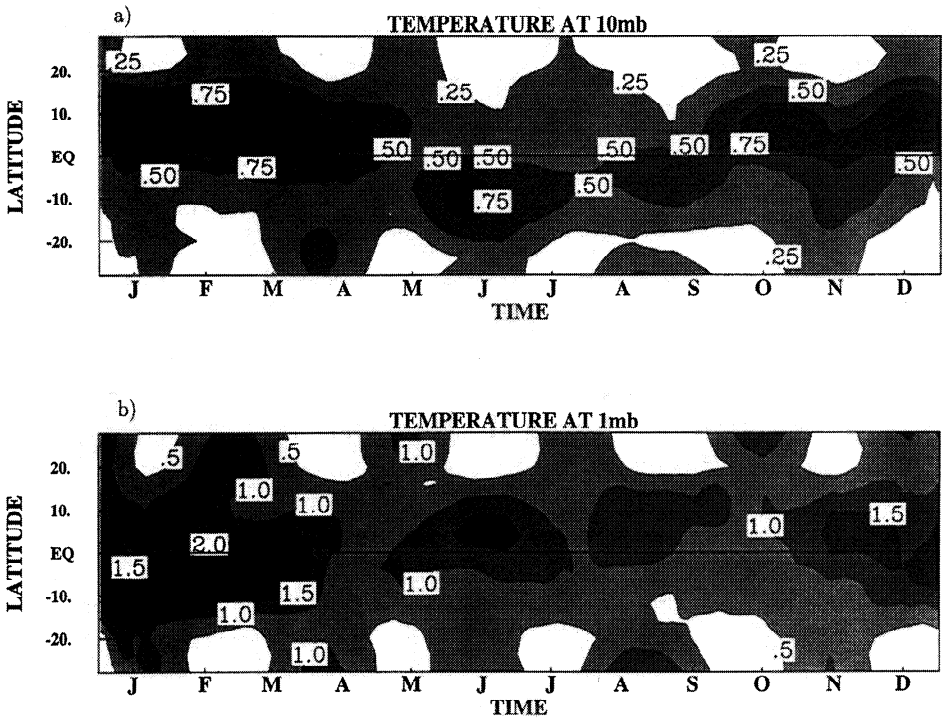


**Figure 8.** Amplitude of the temperature diurnal variation, obtained from daily synoptic maps, averaged over the first three years of the UARS mission. Amplitudes are for temperature at (a) 10 hPa where shading increment is 0.25 K and (b) 1 hPa where shading increment is 0.5 K.

is not understood. It should also be noted that the variation from year to year (not shown) exhibits significant interannual variability. In late 1993 and 1994 the amplitudes are smaller than those in the two preceding years. During 1994 the maximum between February and March is almost absent. *Wu et al.* [1998] provided evidence of similar behavior, which occurs contemporaneously with descending easterlies of the Quasi-Biennial Oscillation. Other observational studies have found similar behavior in mesospheric winds measured by the High Resolution Doppler Imager [*Burrage et al.*, 1995].

## 4. Chemical Variations

In place of instantaneous synoptic structure, which is undersampled by UARS, diurnal variations of chemical species are composited as the mean diurnal variation over a sufficient averaging interval (section 2). Figure 9 shows the composite diurnal variation of $NO_2$ at 5 hPa, as a function of latitude and local time. This composite was obtained by combining all measurements at 2-hour intervals of LT, from January 15, 1992, to March 21, 1992, which span two UARS yaw periods. In the presence of sunlight, nitrogen dioxide is converted into nitric oxide by photolysis,

$$NO_2 + h\nu \rightarrow NO + O(^3P), \tag{3a}$$

or by reaction with atomic oxygen,

$$NO_2 + O \rightarrow NO + O_2. \tag{3b}$$

Nitrogen dioxide is reformed at nighttime when nitric oxide reacts with ozone,

$$NO + O_3 \rightarrow NO_2 + O_2, \tag{3c}$$

or with the hydroperoxy radical,

$$NO + HO_2 \rightarrow NO_2 + OH. \tag{3d}$$

As shown in Figure 9, the mixing ratio of nitrogen dioxide is small during the day but remains nonnegligible (~2 ppbv), whereas it is largest right after sunset (~8 ppbv). Photochemical models [e.g., *Brasseur and Solomon*, 1986] are in agreement with the nighttime values. However, daytime concentrations in models are significantly larger than those in Figure 9. There is also more nitrogen dioxide in the Southern Hemisphere during night at this time of year than there is at the same time in the Northern Hemisphere.

The diurnal cycle in reactions (3a)–(3d) implies that nitric oxide and nitrogen dioxide are converted from one into the other at dusk and dawn. Peak concentrations are therefore expected during opposite phases of the diurnal cycle. Figure 10 shows the composite diurnal variation of nitric oxide for the same period as that in Figure 9. NO is present only in daylight, having a structure that is nearly complementary to that of $NO_2$: When $NO_2$ is small, NO is large, and vice versa. In fact, at each latitude the collective mixing ratios of NO and $NO_2$ remain approximately constant throughout the day, in agreement with the partitioning of $NO_x$ [e.g., *Brasseur and Solomon*, 1986].

The largest extratropical mixing ratios of NO and $NO_2$ are found in the Southern Hemisphere; Northern Hemispheric mixing ratios are ~25% smaller at this time of the year. Nitrogen compounds in the middle

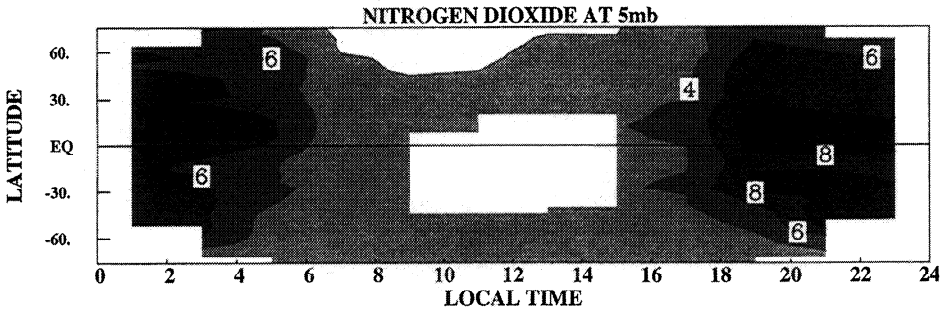


**Figure 9.** Global composite diurnal cycle of nitrogen dioxide (in ppbv) at 5 hPa, averaged from January 15, 1992, to March 21, 1992. The shading increment is 2 ppbv. The composite was obtained by using observations made by CLAES.

atmosphere are, by and large, produced by photolysis of nitrous oxide ($N_2O$). Downwelling in the winter hemisphere introduces air that is lean in nitrous oxide. In fact, monthly averages of nitrous oxide at 5 hPa during solstice (not shown) show zonal mean mixing ratios in the Southern Hemisphere that are larger than those in the Northern Hemisphere. Therefore, at a given height, more nitrogen compounds can be produced through photolysis of $N_2O$ in the summer hemisphere, which is under the influence of upwelling, than in the winter hemisphere, which is under the influence of downwelling.

The composite diurnal variation of chlorine nitrate ($ClONO_2$) is shown in Figure 11 for the same time period as that of Figure 9. Chlorine nitrate is produced at night from the reaction of chlorine monoxide with nitrogen dioxide:

$$ClO + NO_2 + M \rightarrow ClONO_2 + M. \quad (4a)$$

The largest concentrations ($\sim$ 0.5 ppbv) are found near the wintertime polar vortex, where air parcels reside in darkness most of the time. After sunrise, chlorine nitrate is rapidly dissociated to form free chlorine and nitrogen trioxide:

$$ClONO_2 + h\nu \rightarrow Cl + NO_3. \quad (4b)$$

This reaction accounts for the disappearance of $ClONO_2$ during daytime, as well as for a phase that is nearly opposite to chlorine monoxide (see Figure 12). Photochemical models predict the largest concentration of chlorine nitrate just before sunrise, in accord with Figure 11, but with somewhat smaller concentrations of $\sim$0.3-0.4 ppbv [*Brasseur and Solomon*, 1986].

Figure 12 shows the composite diurnal variation of chlorine monoxide at 5 hPa. Chlorine monoxide is produced during the day by the reaction of free chlorine with ozone,

$$Cl + O_3 \rightarrow ClO + O_2, \quad (5)$$

whereas at night it is converted into chlorine nitrate through reaction (4a). The structure of ClO is nearly complementary to that of $ClONO_2$ (Figure 11), in accord with the partitioning of $ClO_x$. The largest mixing ratio of chlorine monoxide ($\sim$0.8 ppbv) is observed during daytime at $\sim$13 LT at northern midlatitudes. Near the equator the concentration of chlorine monoxide is somewhat smaller ($\leq$ 0.4 ppbv), peaking at about the same local time.

There is more chlorine monoxide at this time of year in the Northern Hemisphere than there is in the Southern Hemisphere. The smaller concentration of chlorine monoxide in the Southern Hemisphere during daytime can be understood by recalling that the chlorine and nitrogen families are coupled during the day through the reaction of chlorine monoxide with nitric oxide:

$$ClO + NO \rightarrow Cl + NO_2. \quad (6)$$

Because of this coupling and the higher mixing ratios of nitric oxide in the Southern Hemisphere (Figure 10), reaction (6) implies lower mixing ratios of chlorine monoxide in the Southern Hemisphere. (Chlorine monoxide is also reformed through recombination of free chlorine with ozone (reaction (5)). However, destruction of chlorine monoxide via reaction (6) is twice as fast as its production via reaction (5).)

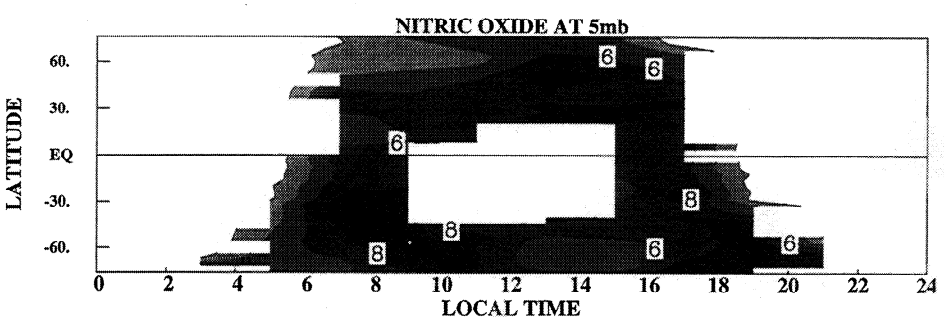


**Figure 10.** As in Figure 9 but for nitric oxide. The shading increment is 2 ppbv. The composite was obtained by using observations made by CLAES.

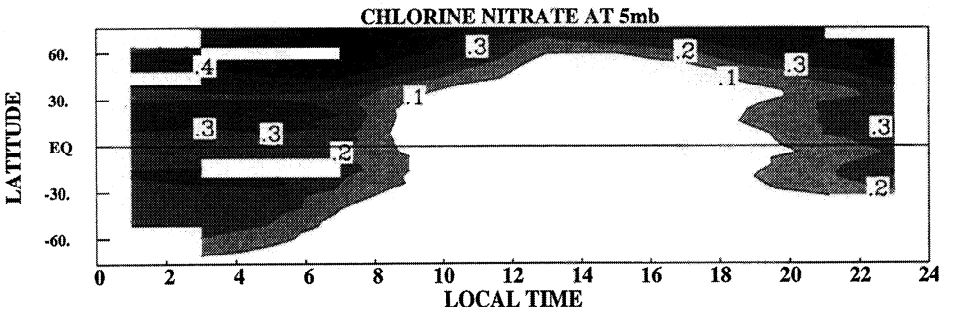


**Figure 11.** As in Figure 9 but for chlorine nitrate. The shading increment is 0.1 ppbv. The composite was obtained by using observations made by CLAES.

## 5. Conclusions

Diurnal variations of dynamical and chemical structure emerge in UARS measurements as prominent features of the middle atmosphere, evident even in the middle and upper stratosphere. The temperature field is smooth enough for diurnal variations to be mapped synoptically. Even when higher harmonics of the diurnal cycle are present, the magnitude of undersampled variability is small in the stratosphere. It should be noted, however, that the diurnal cycle becomes larger at higher levels, with predicted amplitudes in the mesosphere exceeding several tens of degrees [e.g., *Lindzen*, 1967]. Undersampled diurnal variability is then no longer negligible, so the corruption of mapped products at those levels can be substantial.

The UARS data also reveal seasonal changes of the diurnal tide, in which its structure and amplitude vary systematically. The temperature variation maximizes near but off the equator, meandering from one hemisphere to the other according to the time of year. The temperature maximum amplifies near each solstice (i.e., on a semiannual timescale), when it is farthest from the equator. Its meandering about the equator, however, makes the tide's seasonality in either hemisphere annual. Latitudinal excursions of the temperature maximum are largest below 5 hPa, where they track across the equator opposite to the sun. Above 5 hPa, however, they track across the equator with the sun. At sufficient height the temperature maximum converges onto the equator, making the seasonality of the diurnal tide semiannual, as has been noted from other measurements in the upper mesosphere and lower thermosphere [*Vincent et al.*, 1988; *Burrage et al.*, 1995].

Vertical motion associated with the tide displaces tracer mixing ratio surfaces, for example, chemical species with a lifetime much longer than a day. In the lower stratosphere, when ozone is long-lived, the diurnal variation of vertical motion is sufficient to introduce diurnal oscillations of ozone, which are visible in synoptic maps.

For chemical species that are short-lived, abrupt changes occur between day and night. Higher diurnal harmonics introduced by these changes are undersampled by UARS, preventing the instantaneous diurnal variation from being mapped. Composite diurnal variations provide an average diurnal cycle of such species over several UARS yaw periods.

Certain chemical family members recycle one another at different hours of the day. As a result, diurnal variations of some species are complementary. Their combined mixing ratios remain approximately constant, in agreement with the partitioning of those chemical families.

In the middle stratosphere, diurnal variations of $NO_x$ are strongly influenced by the zonal mean distribution of $NO_x$ which in turn is controlled by the mean meridional circulation. The pole-to-pole circulation during solstice brings down air lean in nitrous oxide over the winter hemisphere, but it brings up air rich in nitrous oxide in the summer hemisphere. Therefore comparatively greater concentrations of $NO_x$ are found at extratropical latitudes of the summer hemisphere, where the daily maximum is greatest. The hemispheric asymmetry in $NO_x$ introduced ultimately by the mean meridional circulation is passed into the diurnal cycle of $ClO_x$ through the coupling of these chemical families.

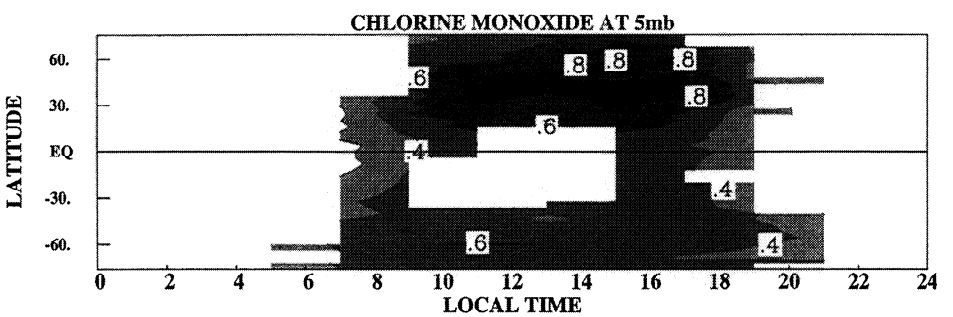


**Figure 12.** As in Figure 9 but for chlorine monoxide. The shading increment is 0.2 ppbv. The composite was obtained by using observations made by MLS.

The results presented here, along with other observations and numerical calculations, provide a fairly consistent picture of diurnal variations in the middle atmosphere. While revealing the basic form and seasonality of diurnal variations, the results also indicate the involvement of diurnal scales beyond those resolved by a single orbiting platform. To fully resolve diurnal behavior, the sampling limits of asynoptic observations must be expanded. This can be accomplished only with multiple orbiting platforms.

**Acknowledgments.** The authors are grateful for constructive comments provided during review. This work was supported by NASA grant NAG5-2852.

## References

Andrews, D. G., J. R. Holton, and C. B. Leovy, *Middle Atmosphere Dynamics*, Academic, San Diego, Calif., 1987.

Brasseur, G., and S. Solomon, *Aeronomy of the Middle Atmosphere*, 2nd ed., D. Reidel, Norwell, Mass., 1986.

Burrage, M. D., M. E. Hagan, W. R. Skinner, D. L. Wu, and P. B. Hays, Long-term variability in the solar diurnal tide observed by HRDI and simulated by the GSWM, *Geophys. Res. Lett.*, *22*, 2641–2644, 1995.

Canziani, P.O., J. R. Holton, E. Fishbein, L. Froidevaux, and J. W. Waters, Equatorial Kelvin waves: A UARS MLS view, *J. Atmos. Sci.*, *51*, 3053–3076, 1994.

Chapman, S., and R. S. Lindzen, *Atmospheric Tides*, Gordon and Breach, Newark, N.J., 1970.

Forbes, J. M., Atmospheric tides, 1, Model description and results for the solar diurnal component, *J. Geophys. Res.*, *87*, 5222-5240, 1982.

Hitchman, M. H., and C. B. Leovy, Diurnal tide in the equatorial middle atmosphere as seen in LIMS temperatures, *J. Atmos. Sci.*, *42*, 557–561, 1985.

Lieberman, R. S., Nonmigrating diurnal tides in the equatorial middle atmosphere, *J. Atmos. Sci.*, *48*, 1112–1127, 1991.

Lindzen, R. S., Thermally driven diurnal tide in the atmosphere, *Q.J.R. Meteorol. Soc.*, *93*, 18–42, 1967.

McLandress, C., G. G. Shepherd, and B. H. Solheim, Satellite observations of thermospheric tides: Results from the wind imaging interferometer on UARS, *J. Geophys. Res.*, *101*, 4093–4114, 1996.

McLandress, C., Seasonal variability of the diurnal tide: Results from the Canadian middle atmosphere general circulation model, *J. Geophys. Res.*, *102*, 29,747–29,764, 1997.

Salby, M. L., Sampling theory for asynoptic satellite observations, I, Spectra, resolution, and aliasing, *J. Atmos. Sci.*, *39*, 2577–2600, 1982a.

Salby, M. L., Sampling theory for asynoptic satellite observations, II, Fast-Fourier synoptic mapping, *J. Atmos. Sci.*, *39*, 2601–2614, 1982b.

Salby, M. L., Asynoptic sampling considerations for wide-field-of-view measurements of outgoing radiation, II, Diurnal and random space-time variability, *J. Atmos. Sci.*, *45*, 1184–1204, 1988.

Salby, M. L., and P. F. Callaghan, Sampling error in climate properties derived from satellite measurements: Consequences of undersampled diurnal variability, *J. of Climate*, *10*, 18–35, 1997.

Salby, M. L., D. L. Hartman, P. L. Bailey, and J. C. Gille, Evidence of equatorial Kelvin modes in Nimbus-7 LIMS, *J. Atmos. Sci.*, *41*, 220–235, 1984.

Sassi, F., and M. L. Salby, Fast Fourier synoptic mapping of UARS data, *J. Geophys. Res.*, *103*, 10,885–10,898, 1998.

Sassi, F., and M. L. Salby, Impact of diurnal variability on UARS synoptic products, *Geophys. Res. Lett.*, in press, 1999.

Solomon, S., R. R. Garcia, and F. Stordal, Transport processes and ozone perturbations, *J. Geophys. Res.*, *90*, 12,981–12989, 1985.

Vincent, R. A., T. Tsuda, and S. Kato, A comparative study of mesospheric solar tides observed at Adelaide and Kyoto, *J. Geophys. Res.*, *93*, 699–708, 1988.

Wu, D. L., C. McLandress, W. G. Read, J. W. Waters, and L. Froidevaux, Equatorial diurnal variations observed in UARS Microwave Limb Sounder temperature during 1991-1994 and simulated by the Canadian Middle Atmosphere Model, *J. Geophys. Res.*, **103**, 8909–8917, 1998.

F. Sassi, Atmospheric Systems and Analysis, 1400 West 122nd Avenue, #101, Westminster, CO 80234. (e-mail: sassi@thunder.asac. org)

M. Salby, Program in Atmospheric and Oceanic Sciences, Campus Box 311, University of Colorado, Boulder, CO 80309.

(Received July 17, 1998; revised October 22, 1998;
accepted October 30, 1998.)